

PREPARATION, ELECTROCHEMISTRY PROPERTIES OF $\text{LiNi}_{0.5-x}\text{Fe}_{0.0485}\text{Mn}_{1.5-y}\text{O}_4$ BY SPRAY-DRY METHOD WITH DIFFERENT Mn/Ni RATIOS

L. ZHOU*, W. LI, L. WAN

Central Academe, Shanghai Electric Group. Co., Ltd, Shanghai, [200433], China

$\text{LiNi}_{0.5}\text{Mn}_{1.5}\text{O}_4$ is considered to be one of the most promising cathode material for next generation high-energy density secondary lithium batteries because of its high theoretical specific capacity of $146.7 \text{ mA h g}^{-1}$ and high theoretical specific energy of 650 W h kg^{-1} . In this work, $\text{LiNi}_{0.5-x}\text{Fe}_{0.0485}\text{Mn}_{1.5-y}\text{O}_4$ with different Mn/Ni ratios were prepared via spray-dry process by controlling reaction conditions. The results show that $\text{LiNi}_{0.5-x}\text{Fe}_{0.0485}\text{Mn}_{1.5-y}\text{O}_4$ has good crystallinity, good conductivity and less impurities with excellent electrochemical properties. The electrochemical tests show that the $\text{LiNi}_{0.485}\text{Fe}_{0.0485}\text{Mn}_{1.475}\text{O}_4$ sample delivers a high initial discharge capacity of 128 mA h g^{-1} and a good cycling stability (reversible discharging capacity of 124 mA h g^{-1} with a capacity retention of 95% in 200 cycles and approximately 124 mA h g^{-1} in 300 cycles operated at 1 C rate).

(Received April 3, 2020; Accepted August 20, 2020)

Keywords: Lithium nickel manganese oxide; Fe doping; Mn/Ni ratios; Cathode material

1. Introduction

In recent years, the huge demands for energy has motivated the development of high-energy density lithium-ion battery materials. Spinel-like $\text{LiNi}_{0.5}\text{Mn}_{1.5}\text{O}_4$ has become one of the most promising candidate for lithium-ion batteries because of its lower toxicity, lower cost, and higher theoretic capacity [1, 2]. Compared to the traditional cathode material, $\text{LiNi}_{0.5}\text{Mn}_{1.5}\text{O}_4$ exhibits higher discharge specific capacity and rate performance with plateaus near 4.8 V vs. Li^+/Li , which can endow the battery with higher working voltage, energy and power density. The theoretical capacity of $146.7 \text{ mA h g}^{-1}$ and the energy density of 650 W h kg^{-1} have laid a solid foundation for the material to be popularized and applied. At present, $\text{LiNi}_{0.5}\text{Mn}_{1.5}\text{O}_4$ has been extensively investigated and considered as one of the most promising cathode materials for next generation lithium-ion batteries [3, 4].

Various of preparing methods have been extensively applied to synthesis $\text{LiNi}_{0.5}\text{Mn}_{1.5}\text{O}_4$ sample. Such as solid phase method [5, 6], co-precipitation method [7, 8], sol-gel method [9, 10], spray pyrolysis method [11], hydrothermal / solvothermal method [12] and molten salt method [13]. Different synthetic routes, specific additives and surfactants will directly affect the crystal growth and form different morphologies. Recent studies have shown that the morphology of cathode particles will have a profound impact on its electrochemical properties [14, 15]. In this

* Corresponding author: zhoulun@shanghai-electric.com

paper, $\text{LiNi}_{0.5-x}\text{Fe}_{0.0485}\text{Mn}_{1.5-y}\text{O}_4$ ($0 < x+y < 0.0485$) cathode materials with different Mn/Ni ratios were prepared by spray-drying method. Their structure, morphology and electrochemical properties were characterized.

Compared with the traditional solid phase method, the spray-drying method can ensure that the raw materials are atomically mixed before sintering, making the doped ions easier to enter the lattice and achieve the Ni/Mn substitution. At the same time, the substitution of Ni and Mn by Fe can inhibit the formation of impurity phases such as $\text{Li}_x\text{Ni}_{1-x}\text{O}$ on one hand, and make the crystal structure transform from space group $P4_332$ to better performance $Fd3m$ on the other hand [16, 17]. This structural transformation is believed to relate to the increase of lithium-ion diffusion coefficient, thus effectively improving the electronic and ionic conductivity of the material [18]. In addition, some recent studies [19] have also pointed out that Fe has self-segregation effect, which can enrich more on the surface of the material and make the surface of the material poor in Ni, thus effectively inhibiting the oxidation and decomposition of the electrolyte, thereby improving the cyclic stability of the material.

In this paper, we attempt to discuss the structural and performance changes of materials with different Mn/Ni ratios after Fe doping into different sites. In order to investigate this change systematically, we prepared a series of materials doped with the same amount of Fe at different sites. For comparison, we also prepared $\text{LiNi}_{0.5}\text{Mn}_{1.5}\text{O}_4$ as cathode material without Fe doping. The results show that Fe can enter the spinel structure well after substituting Ni and Mn simultaneously. There are no impurities in the XRD results, and the edges and corners of Fe-doped materials become smooth in TEM photos. We find that when the Mn/Ni ratio approaches 3 after Fe doping into Ni and Mn sites, the substitution performs the highest capability and best cyclic stability.

2. Experimental

2.1. Preparation of $\text{LiNi}_{0.5}\text{Mn}_{1.5}\text{O}_4$ and $\text{LiNi}_{0.5-x}\text{Fe}_{0.0485}\text{Mn}_{1.5-y}\text{O}_4$ with different Mn/Ni ratios

The preparation process is shown in Fig. 1. The raw materials Li_2CO_3 , NiO, Mn_3O_4 , $\text{Fe}(\text{NO}_3)_3 \cdot 9\text{H}_2\text{O}$ (AR, analytical purity) were separately weighed by the stoichiometric ratios of $\text{LiNi}_{0.5}\text{Mn}_{1.5}\text{O}_4$, $\text{LiNi}_{0.5}\text{Fe}_{0.0485}\text{Mn}_{1.46}\text{O}_4$, $\text{LiNi}_{0.485}\text{Fe}_{0.0485}\text{Mn}_{1.475}\text{O}_4$ and $\text{LiNi}_{0.47}\text{Fe}_{0.0485}\text{Mn}_{1.485}\text{O}_4$ (Li_2CO_3 has certain volatility, Li source excess 3%) and dispersed in a certain amount of water to form a water solution with solid content of 20% and milled in a sand mill for 2 h. Crushing and mixing at nanometer level to achieve uniform dispersion of raw materials at molecular or atomic level according to the stoichiometric ratio. Then, the mixed solution was dried by spray drying apparatus, and the spherical precursor compound powder at the molecular level was obtained. Finally, the precursor powder was calcined in muffle furnace, and then treated at low temperature at 450 °C for 2 h, making the raw materials uniform decomposition and react completely. Next, heat treatment at high temperature at 900 °C for 12 h ensures the thoroughness of crystallization and the integrity of crystallinity in the process of crystal formation, avoids some defects in octahedral spinel structure of the obtained material, which affects the de-intercalation of lithium ions. Lastly, annealing at 700 °C for 6 h at low temperature, preventing the formation of nickel-rich phase component (NiO or $\text{Li}_x\text{Ni}_{1-x}\text{O}$) during high temperature, which reduces the generation of impurity phase and improves the purity of the product.

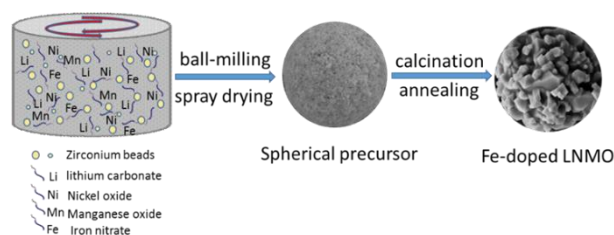


Fig. 1. Preparation illustration of lithium nickel manganese oxides with Fe-doping.

Sample	Mn/Ni	D10(um)	D50(um)	D90(um)	BET
$\text{LiNi}_{0.5}\text{Mn}_{1.5}\text{O}_4$	3	9.48	19.7	39.6	0.8034
$\text{LiNi}_{0.5}\text{Fe}_{0.0485}\text{Mn}_{1.46}\text{O}_4$	2.92	5.92	12.5	26.2	1.1127
$\text{LiNi}_{0.485}\text{Fe}_{0.0485}\text{Mn}_{1.475}\text{O}_4$	3.04	6.52	13.4	26.2	1.1102
$\text{LiNi}_{0.47}\text{Fe}_{0.0485}\text{Mn}_{1.485}\text{O}_4$	3.16	7.8	15.5	30.2	0.8985

2.2. Morphological characterization and electrochemical measurements

The as-prepared composites were characterized by powder XRD patterns (Bruker D8 Advance, Cu $K\alpha$ radiation, $\lambda = 1.5406 \text{ \AA}$). The morphologies and microstructure of the composites were investigated using scanning electron microscopy (SEM JEOL JSM-6390) and transmission electron microscopy (TEM, JEM-2100F). Nitrogen adsorption isotherms were measured at 77 K on a Quantachrome Autosorb-1-MP (Quantachrome, USA).

The electrodes were prepared from a mixture of 92 wt. % of active material, 5 wt. % of super p and 3 wt. % of PVDF binder in NMP (N-methyl-2-pyrrolidone), which served as the dispersant. The slurries were uniformly cast onto aluminum foil substrate using a doctor blade. After the NMP was evaporated, the cathode was subsequently pressed into disks with a diameter of 10 mm and then dried under vacuum at 110 °C for 12 h. The test cell was assembled in an argon-filled glove box with a Li counter electrode and a Celgard 2300 sheet as separator. The electrolyte employed was 1 M LiPF_6 in a mixture of EC/DEC/DMC ((v:v:v = 1:1:1)) solution, and FEC as the additive. The charge-discharge measurements were carried out at certain current density with a voltage range of 3.5–5.0 V vs. Li/Li^+ using a Land Cycler (CT2001A, Wuhan Jinnuo Electronic Co. Ltd.). The specific capacity values in this work were calculated on the basis of active mass.

3. Results and discussion

3.1. Morphology and structure of doping or undoping $\text{LiNi}_{0.5}\text{Mn}_{1.5}\text{O}_4$ composites

The particle size and specific surface area of four samples were obtained by Malvine test and nitrogen adsorption/desorption isotherm curve, as shown in Fig. 2. It can be seen from the figure that the particle size of the samples doped with Fe is obviously smaller than that of the

sample without Fe, and the specific surface area of the samples with Fe doping are larger than that of the sample without Fe. We speculate that the doping of Fe into the lattice of the material can inhibit the growth of the material particles. For Fe-doped samples, the particle size increases slightly with the increase of Mn/Ni ratio, and the specific surface area decreases. It is generally believed that high specific surface area is conducive to the transport of lithium ions and the infiltration of electrolyte in materials, thus improving the electrochemical properties of materials.

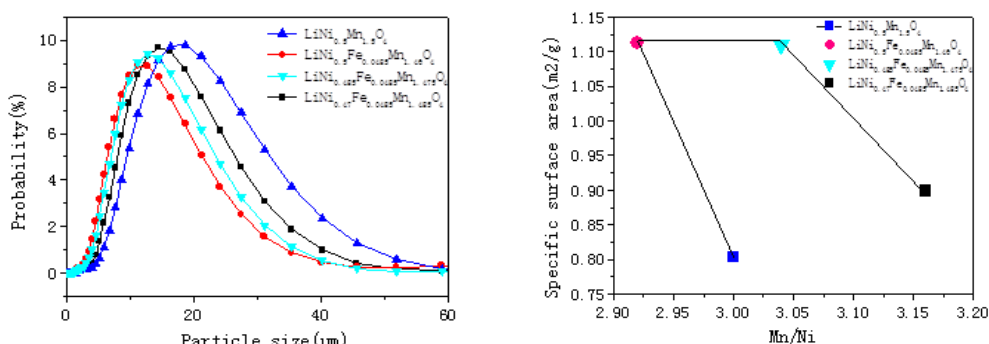


Fig. 2. Particle size distribution and specific surface area of lithium nickel manganese oxides with or without Fe-doping.

The typical morphology and particles size distribution of the two samples with/without Fe-doping were investigated by SEM, and the images are shown in Fig. 3 (a1, a2) , two samples are composed of spinel octahedral secondary particles, despite some minor aggregation, the particles still show a clear loose morphology and uniform distribution. The distribution of elements in lithium nickel manganese was also measured by EDS, which can be observed in Fig. 3 (b1, b2). It can be seen that Ni/Mn elements are dispersed uniformly in the entire detecting range. Similarly, the EDS result reveals that the Fe elements has been successfully introduced into lithium nickel manganese, and dispersed uniformly in the $\text{LiNi}_{0.485}\text{Fe}_{0.0485}\text{Mn}_{1.475}\text{O}_4$ particles, as shown in Fig. 3 (b2).

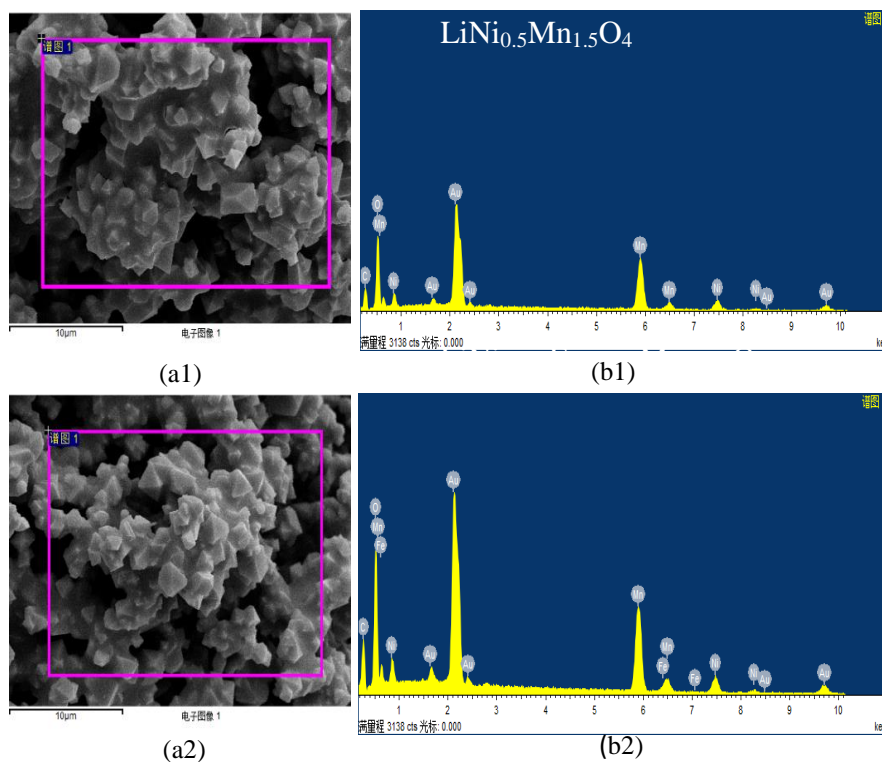


Fig. 3. SEM images and EDS of $\text{LiNi}_{0.5}\text{Mn}_{1.5}\text{O}_4$ (a1, b1) and $\text{LiNi}_{0.485}\text{Fe}_{0.0485}\text{Mn}_{1.475}\text{O}_4$ (a2, b2).

In the TEM image as shown in Fig. 4 (a1 and b1), It can be observed that the surface of Fe-doping sample is more smooth, which is consistent with the previous particle size distribution speculation, that is, the doping of Fe into the lattice of materials can inhibit the growth of materials particles, especially edges and corners. Fig. 4 (a 2 and b2) show the HRTEM images of the lattice fringe, of which the measured d_{hkl} is around 0.47 nm, corresponding to the $\{111\}$ interplanar spacing. This corresponds to the (111) crystal spacing in the XRD measurements. It further shows that both the samples with/without Fe-doping are octahedral with $[111]$ exposed crystal faces [20].

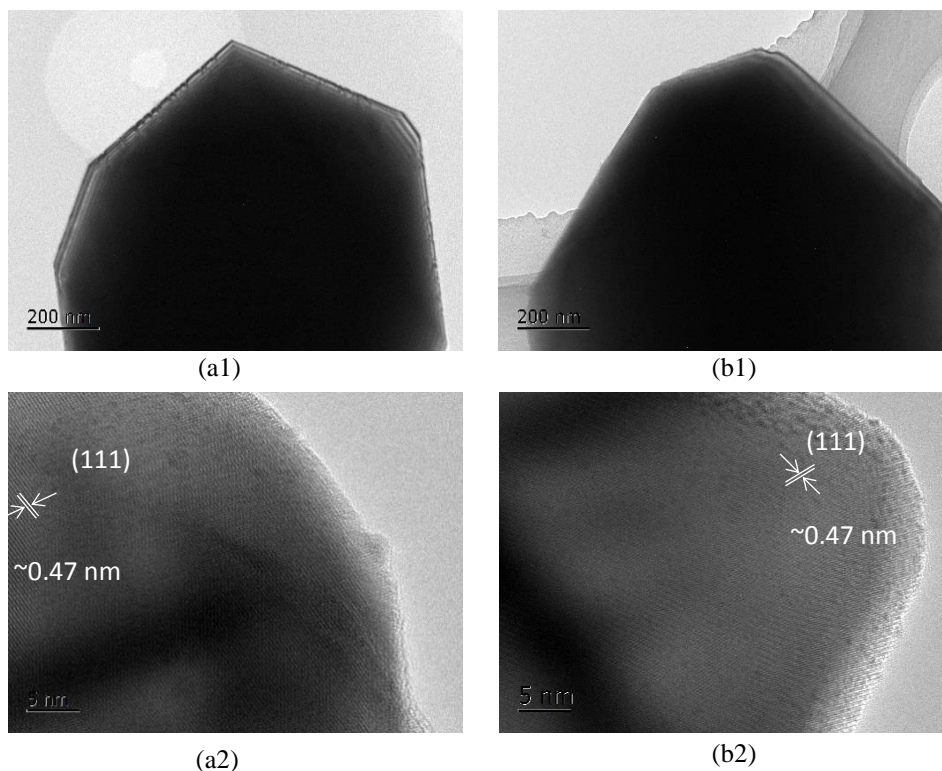


Fig. 4. TEM images of $\text{LiNi}_{0.5}\text{Mn}_{1.5}\text{O}_4$ (a1, a2) and $\text{LiNi}_{0.485}\text{Fe}_{0.0485}\text{Mn}_{1.475}\text{O}_4$ (b1, b2).

The crystal structure of the samples was characterized by X-ray diffraction (XRD) with $\text{Cu K}\alpha$ radiation. Fig. 5 shows the XRD spectra of $\text{LiNi}_{0.5}\text{Mn}_{1.5}\text{O}_4$ and $\text{LiNi}_{0.485}\text{Fe}_{0.0485}\text{Mn}_{1.475}\text{O}_4$ samples. It can be seen from the figure that although both of them can well correspond to the standard JCPDS card 80-2162 of spinel structure of $\text{LiNi}_{0.5}\text{Mn}_{1.5}\text{O}_4$, the obvious diffraction peaks located at approximately 37° and 44° of $\text{Li}_x\text{Ni}_{1-x}\text{O}$, which is a common impurity phase derived from oxygen vacancy during the high temperature (over 750°C) synthesis for $\text{LiNi}_{0.5}\text{Mn}_{1.5}\text{O}_4$ [21], can be observed in the sample of undoping Fe and disappeared in the sample of doping Fe, which indicates that Fe can fuse well into the crystal lattice of spinel $\text{LiNi}_{0.5}\text{Mn}_{1.5}\text{O}_4$ and inhibit the formation of impure phase of Ni oxide. This may be related to the particle size distribution in the mixing process of sand mill. We find that the particle size of slurry obtained by sand grinding at the same time is smaller after adding iron nitrate in raw material, which makes the precursor in the calcination process, on one hand, uniform contact and more sufficient reaction because of the small particle size, avoiding the formation of nickel-rich phase due to uneven element. On the other hand, because of the small particle size of the reactant, the phase synthesis can be faster, and the impurity phase due to partial enrichment of Ni is avoided.

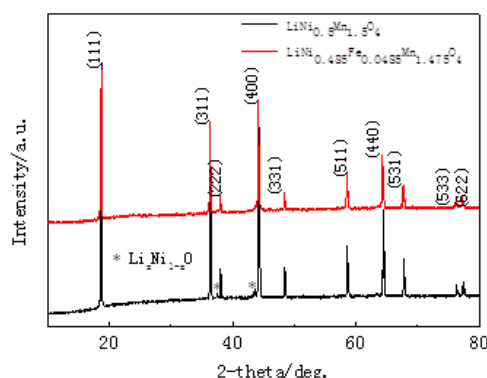


Fig. 5. XRD pattern of $\text{LiNi}_{0.5}\text{Mn}_{1.5}\text{O}_4$ and $\text{LiNi}_{0.485}\text{Fe}_{0.0485}\text{Mn}_{1.475}\text{O}_4$.

3.2. Electrochemical performance of doping or undoping $\text{LiNi}_{0.5}\text{Mn}_{1.5}\text{O}_4$ samples

The charge-discharge curves of four samples at 1 C within a cut-off voltage window of 3.5–5 V are shown in Fig. 6. Two typical characteristic plateaus were observed in the discharge profile in all samples, ~ 4.7 V and ~ 4.0 V respectively. The upper plateau (~ 4.7 V) split into two smaller platforms, corresponding to $\text{Ni}^{4+}/\text{Ni}^{3+}$ and $\text{Ni}^{3+}/\text{Ni}^{2+}$ pairs, respectively. For the undoping $\text{LiNi}_{0.5}\text{Mn}_{1.5}\text{O}_4$, the splitting platforms are 4.68 and 4.66 V, with a difference of 0.02 V. For the Fe-doping $\text{LiNi}_{0.5}\text{Mn}_{1.5}\text{O}_4$, the splitting platforms are 4.68 and 4.61 V. The difference between the two platforms increases to 0.07 V. These results show that the substitution of Fe for Ni and Mn affects the embedding/detachment behavior of Li^+ in the charge-discharge process. The plateau in the 4.0 V region corresponds to the redox reaction of $\text{Mn}^{3+}/\text{Mn}^{4+}$. The capacity of the plateau increases when Fe replaces Ni and Mn, which indicates that with the appearance of Fe, the crystal structure of the material changes. The space group changes from $P4_332$ to $Fd3m$, and the content of Mn^{3+} in the sample increases. Similar phenomena occur after Co replaces $\text{LiNi}_{0.5}\text{Mn}_{1.5}\text{O}_4$ [22]. It can be inferred that the increase of plateau capacity of 4.0 V caused by the replacement of Ni and Mn by Fe is also related to the increase of oxygen defect. The Fe-doping material contains a certain amount of Mn^{3+} , which greatly reduces the transfer resistance of the material's ionic conductors and improves the electrochemical properties of the material, as shown in Fig. 6.

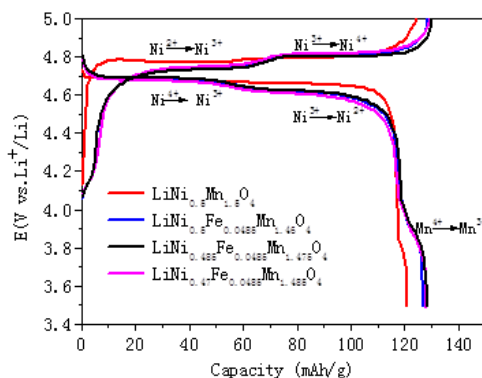


Fig. 6. The charge-discharge profiles of $\text{LiNi}_{0.5}\text{Mn}_{1.5}\text{O}_4$, $\text{LiNi}_{0.5}\text{Fe}_{0.0485}\text{Mn}_{1.46}\text{O}_4$, $\text{LiNi}_{0.485}\text{Fe}_{0.0485}\text{Mn}_{1.475}\text{O}_4$ and $\text{LiNi}_{0.47}\text{Fe}_{0.0485}\text{Mn}_{1.485}\text{O}_4$.

Fig. 7 shows the cycling performance of four samples for 500 cycles at 1 C. The initial discharge capacity were 120.7, 126.2, 128.6 and 128.4 mA h/g, respectively. The discharge capacity of $\text{LiNi}_{0.5}\text{Mn}_{1.5}\text{O}_4$ increased gradually in the first five cycles, and increased to 125 mA h/g at the fifth cycle, then began to decay. After 500 cycles, the discharge capacity was 17.5 mA h/g, which is 14.5% of the initial capacity. There was no similar phenomenon in Fe-doping $\text{LiNi}_{0.5}\text{Mn}_{1.5}\text{O}_4$ materials. $\text{LiNi}_{0.5}\text{Fe}_{0.0485}\text{Mn}_{1.46}\text{O}_4$, $\text{LiNi}_{0.485}\text{Fe}_{0.0485}\text{Mn}_{1.475}\text{O}_4$ and $\text{LiNi}_{0.47}\text{Fe}_{0.0485}\text{Mn}_{1.485}\text{O}_4$ exhibit stable cyclic performance with capacity retention rates of 76.8%, 91.6% and 55.9% respectively after 500 cycles. The capacity decay rate of the samples with Fe doping is lower than that of the undoping $\text{LiNi}_{0.5}\text{Mn}_{1.5}\text{O}_4$ material, which indicates that the cyclic performance of the samples can be improved effectively by substituting Fe for Ni and Mn. This is mainly attributed to the following aspects. Firstly, Fe replaces Ni and Mn at the same time, which makes the material structure change into $Fd3m$ type with better performance. The material contains a small amount of Mn^{3+} , which greatly reduces the transfer resistance of the material's ionic conductor and improves the electrochemical performance of the material [23]. Secondly, the particle size of Fe-doping samples is smaller than that of non-doping samples, which can shorten the Li^+ ion diffusion distance [21]. As shown in XRD, Fe can well enter the spinel lattice of the original materials and inhibit the formation of Ni oxide impurities. Thirdly, due to the self-segregation effect, Fe is more concentrated on the surface of materials, making the surface of Fe-doping samples is in the state of poor Ni, so the oxidation and decomposition of electrolyte are effectively inhibited, and the cycling performance of the material is improved [19]. The samples of $\text{LiNi}_{0.485}\text{Fe}_{0.0485}\text{Mn}_{1.475}\text{O}_4$ with Mn/Ni ratio of 3.04 have the best cyclic stability. Besides the above reasons, it also depends on the high specific surface area and the existence of trivalent manganese ions. Generally speaking, high specific surface area is conducive to the transport of lithium ions and the infiltration of electrolyte, thus improving the electrochemical properties of materials. For the other Fe-doping samples, the Mn/Ni ratios are 2.92 and 3.16, respectively. When the amount of nickel is excessive or manganese is excessive, the capacity both decreases dramatically after 300 cycles. The reason may be that the higher nickel concentration is easier to catalytic decomposition of electrolytes, especially at high potential, while the higher manganese concentration is easier to dissolve into the electrolyte, resulting in the destruction of the internal structure of the material, which leads to the large polarization in the later cycles and decrease of cycle stability.

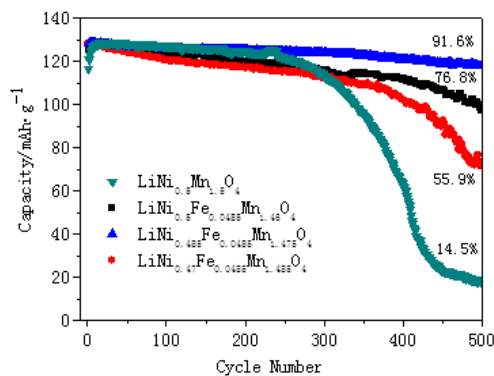


Fig. 7. Cyclic performance of $\text{LiNi}_{0.5}\text{Mn}_{1.5}\text{O}_4$, $\text{LiNi}_{0.5}\text{Fe}_{0.0485}\text{Mn}_{1.46}\text{O}_4$, $\text{LiNi}_{0.485}\text{Fe}_{0.0485}\text{Mn}_{1.475}\text{O}_4$ and $\text{LiNi}_{0.47}\text{Fe}_{0.0485}\text{Mn}_{1.485}\text{O}_4$.

4. Conclusions

LiNi_{0.5}Mn_{1.5}O₄ as cathode material for spinel lithium-ion batteries has many advantages, such as high working voltage, high specific capacity, high energy density, environmentally friendly and three-dimensional lithium-ion diffusion channels. It has great potential application value in electric vehicles, energy storage and other fields in the future. In this paper, LiNi_{0.5-x}Fe_{0.0485}Mn_{1.5-y}O₄ ($0 < x+y < 0.0485$) with loose structure were prepared by spray-drying method. The structure, morphology and electrochemical properties of the cathode material were characterized. Compared with the traditional solid phase method, the spray-drying method can ensure that the raw materials are atomically mixed before sintering, which makes the doped ions easier to enter the lattice and achieve Ni/Mn substitution.

At the same time, Ni and Mn substituted by Fe can inhibit the formation of impurities such as Li_xNi_{1-x}O on the one hand, and change the crystal structure of materials from space group *P4₃32* to better performance *Fd3m* on the other hand. This structural transformation brings about an increase in the chemical diffusion coefficient of lithium ions, thus effectively improving the electronic and ionic conductivity of materials. In this paper, the essential defects of LiNi_{0.5}Mn_{1.5}O₄ are remedied to a certain extent by the improvement of synthesis method and material modification. Especially when Mn/Ni ratio is 3.04, LiNi_{0.485}Fe_{0.0485}Mn_{1.475}O₄ material has high capacity and excellent long cycle stability. It is hoped that in the future, while improving the electrochemical properties of LiNi_{0.5}Mn_{1.5}O₄ cathode, its working mechanism can be further explored and further studied for people. The development of LiNi_{0.5}Mn_{1.5}O₄ material will provide some guidance for accelerating the commercialization of high specific energy lithium-ion battery cathode.

References

- [1] E. S. Lee, K. W. Nam, E. Hu et al., *Chemistry of Materials* **24**, 3610 (2012).
- [2] K. R. Chemelewski, D. W. Shin, W. Li et al., *Journal of Materials Chemistry A* **1**, 3347 (2013).
- [3] Q. M. Zhong, A. Bonakdaipour, M. J. Zhang, Y. Gao, J. R. Dahn, *Journal of the Electrochemical Society* **144**, 205 (1997).
- [4] X. Y. Feng, C. Shen, X. Fang et al., *J. Alloys Compd.* **509**, 3623 (2011).
- [5] T. Ohzuku, K. Ariyoshi, S. Yamamoto, *J. Ceram. Soc. Jpn.* **110**, 501 (2002).
- [6] B. J. Hwang, Y. W. Wu, M. Venkateswarlu, M. Y. Cheng, R. Santhanam, *J. Power Sources* **193**, 828 (2009).
- [7] J. Liu, A. Manthiram, *J. Electrochem. Soc.* **156**, A833 (2009).
- [8] J. Hassoun, K. S. Lee, Y. K. Sun, B. Scrosati, *J. Am. Chem. Soc.* **133**, 3139 (2011).
- [9] T. Yang, K. Sun, Z. Lei, N. Zhang, Y. Lang, *J. Alloys Compd.* **502**, 215 (2010).
- [10] M. Kunduraci, G. G. Amatucci, *Electrochim. Acta* **53**, 4193 (2008).
- [11] U. Lafont, A. Anastasopol, E. Garcia-Tamayo, E. Kelder, *Thin Solid Films* **520**, 3464 (2012).
- [12] Cao, A. Manthiram, *Phys. Chem. Chem. Phys.* **14**, 6724 (2012).
- [13] S. X. Zhao, X. F. Fan, Y. F. Deng, C. W. Nan, *Electrochim. Acta* **65**, 7 (2012).
- [14] Y. M. Liu, F. Cao, B. L. Chen, X. Z. Zhao, S. L. Suib, H. L. W. Chan, J. K. Yuan, *J. Power Sources* **206**, 230 (2012).
- [15] D. H. Hu, S. X. Zhao, Y. F. Deng, C. W. Nan, *J. Mater. Chem. A* **1**, 14729 (2013).
- [16] G. B. Zhong, Y. Y. Wang, X. J. Zhao, Q. S. Wang, Y. Yu, C. H. Chen, *J. Power Sources* **216**,

368 (2012).

- [17] H. L. Wang, H. Xia, M. O. Lai, L. Lu, *Electrochem. Commun.* **11**, 1539 (2009).
- [18] J. H. Kim, S. T. Myung, C. S. Yoon et al., *Chemistry of materials* **16**, 906 (2004).
- [19] J. Liu, A. Manthiram, *The Journal of Physical Chemistry C* **113**, 15073 (2009).
- [20] H. B. Lin, Y. M. Zhang, H. B. Rong, S. W. Mai, J. N. Hu, Y. H. Liao, L. D. Xing, M. Q. Xu, X. P. Li, W. S. Li, *J. Mater. Chem. A* **2**, 11987 (2014).
- [21] J. Deng, Y. Xu, L. Xiong, *Journal of Alloys and Compounds* **677**, 18 (2016).
- [22] A. Ito, D. Li, Y. Lee, *Journal of Power Sources* **185**, 1429 (2008).
- [23] R. Santhanam, B. Rambabu, *J. Power Sources* **195**, 5442 (2010).